

Authors' response — In a recent paper¹, we demonstrated a new technique for spatially imaging the vectorial properties of optical near fields. In the preceding comment², Gersen *et al.* speculate that only some bounding box, instead of a local elliptical polarization state, is measured and that this measurement depends strongly on the shape of the tip. This is incorrect. In our experiment, the orientation and shape of an arbitrary local elliptical polarization is reconstructed and this reconstruction is independent of the shape of the tip, provided that the polarizability tensor of the tip is characterized.

The general elliptical polarization in the x - z plane can be written as³:

$$\begin{aligned} \mathbf{E}_{\text{local}} &= (E_x, E_z) \\ &= \text{Re}[a_1 \exp(-i\omega t - i\delta_1), \\ &\quad a_2 \exp(-i\omega t - i\delta_2)], \\ &\quad a_1, a_2 > 0. \end{aligned} \quad (1)$$

Here Re means the real part and ω is the angular frequency. Equation (1) in ref. 2 is incorrect. For a two-dimensional plane harmonic wave with wave vector $\mathbf{k} = (k_x, k_z)$, the field should read $\mathbf{E}(\mathbf{r}) = \text{Re}[a_1 \exp[i(\mathbf{k} \cdot \mathbf{r} - \omega t + \delta_1)], a_2 \exp[i(\mathbf{k} \cdot \mathbf{r} - \omega t + \delta_2)]]$, with $a_1, a_2 > 0$ and $\mathbf{r} = (x, y)$. The plane-wave approximation made in ref. 2 is of course not appropriate to describe the locally varying field intensities in our experiments.

In our experiments, a dipole scatterer gives a scattered field $\mathbf{E}_s \propto \mathbf{p} \cdot \mathbf{E}_{\text{local}}$, where \mathbf{p} is the polarizability tensor of the scatterer. The scattered light is then passed through a linear polarizer, performing a projection $\mathbf{E}_p \propto \mathbf{P} \cdot \mathbf{E}_s$. Here \mathbf{P} is given by, $\mathbf{P} = (\cos\theta, \sin\theta)$, where θ is the polarizer angle from the x axis. We measure the time-averaged intensity, $I \propto \langle |\mathbf{P} \cdot \mathbf{E}_s|^2 \rangle$ by rotating the detection polarizer in 10° steps (Fig. 1a). Polar diagrams of $\sqrt{I}(\theta)$ enable us to determine the polarization state of the scattered field. The elliptical polarization state of the original local field $\mathbf{E}_{\text{local}}$ is then reconstructed by performing a back-transformation on the scattered field, $\mathbf{p}^{-1} \cdot \mathbf{E}_s$.

To see how the polar diagrams determine the major axis of the elliptical polarization, we assume an isotropic scatterer:

$$\mathbf{P} = \begin{pmatrix} 1 & 0 \\ 0 & 1 \end{pmatrix}.$$

The measured intensity is then written as:

$$I(\theta) = \langle |\mathbf{P} \cdot \mathbf{E}_s|^2 \rangle = a_1^2 \cos^2 \theta + a_2^2 \sin^2 \theta + 2a_1 a_2 \cos(\delta_1 - \delta_2) \sin \theta \cos \theta, \quad (2)$$

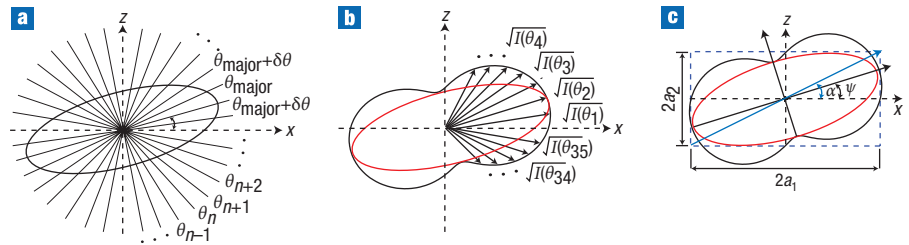


Figure 1 Schematics for the detection and analysis of an elliptically polarized scattered field. **a**, The electric field of the scattered light (represented as a rotated ellipse in the x - z plane) is traced by rotating a linear polarizer in front of the detector by 360° , in steps of 10° . From symmetry considerations, it is easy to see that the maximum intensity of light passing through the polarizer should appear at the polarizer angle equal to the major-axis angle $\theta = \theta_{\text{major}}$; if the maximum were to appear at a different angle, there would be another maximum at the mirror-symmetry angle at the other side of $\theta = \theta_{\text{major}}$ (n is an integer.) **b**, Square-rooted intensities from the polarizer are plotted for every polarization angle. This is the experimental procedure performed to make the polar plot at every spatial position. **c**, ψ is the angle from the major-axis angle to the x axis and α is the angle of the boxing corner. The angle (θ_{max}) of the measured intensity maximum corresponds to ψ and the square-rooted maximum intensity is identical to half of the major-axis length. A wrong experiment using only two fixed orthogonal polarization angles or a few selected angles could yield the boxing angle α of the 'box', and the size of the error would depend on the specific choice of the two orthogonal angles and the ellipticity.

as illustrated in Fig. 1b. Equation (2) can be compared with a similar expression in refs 4 and 5 for a single-molecule case. By taking the derivative of equation (2), we get the angle θ_{max} , where the measured intensity is a maximum:

$$\tan 2\theta_{\text{max}} = \frac{2a_1 a_2 \cos(\delta_1 - \delta_2)}{a_1^2 - a_2^2}. \quad (3)$$

On the other hand, the major axis of an elliptical polarization occurs at an angle³:

$$\tan 2\psi = \frac{2a_1 a_2 \cos(\delta_1 - \delta_2)}{a_1^2 - a_2^2}. \quad (4)$$

Comparing equations (3) and (4), reveals that the experimental polar plots readily correspond to the major axes of local elliptical polarizations not only in direction, but also in magnitude. In the same way, the orientation and magnitude of the minor axis is obtained, thus the ellipticity is fully reconstructed. Polar plots offer an efficient way of tracing the elliptical polarization: a polarization-resolved interferometry experiment⁶ combined with a scattering tip could achieve the same effect, with additional phase information. It is clear that in our experiments, the boxing angle (α) represented in Fig. 1c, is completely irrelevant.

In Fig. 2, we illustrate, with actual experimental data, how we perform the vector-field mapping. We first characterize the tip for 36 incoming far-field polarizations by taking the polar plots of the scattered light at each

incoming polarization angle (Fig. 2a). The polarization tensor is then obtained by fitting the outer rim of such polar plots to an ellipse (Fig. 2b). In the tip used here, the principal axes are rotated by about 6° from the x and z axes, so that in the laboratory frame, it can be written as:

$$\mathbf{P} = \begin{pmatrix} 1.35 & 0.036 \\ 0.036 & 1 \end{pmatrix}.$$

The polar plot of the scattered field, \mathbf{E}_s , from a specific near-field position is shown in Fig. 2c, where the dots represent actual data points. The local polarization $\mathbf{E}_{\text{local}}$ is obtained by taking the back-transformation. Our vector-field mapping shown in Fig. 1d,e, Fig. 2d-f and Fig. 3c,d of ref. 1 followed these procedures. We have represented the elliptical polarization state of the local field, $\mathbf{E}_{\text{local}}$, by a linear field vector along the long axis of the polarization ellipse at several hundreds of positions in the two-dimensional spatial scans. This would of course be meaningless for circularly polarized fields. In our measurements, however, the ellipticity was comparatively large, so that the chosen representation is indeed meaningful.

The authors also claim that our single-slit experiments show errors because of poor tip characterization or even the tip breaking in the middle of the scan. This is also untrue. Our tips are well characterized as shown here in Fig. 2a and b and also in ref. 1. The experimental results and theory agree qualitatively: both show slower decay of E_x and a rotation of the field vector outside

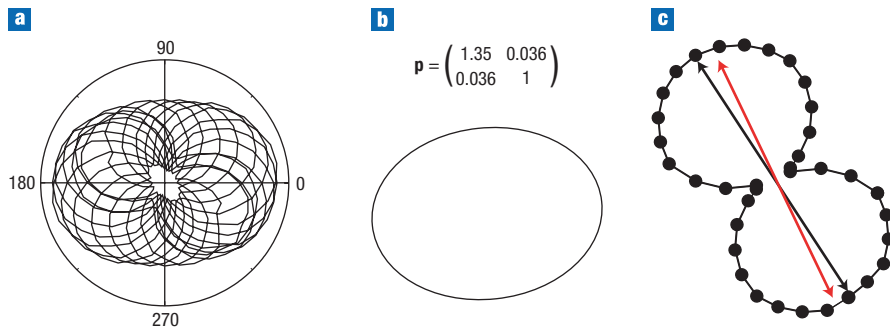


Figure 2 Tip characterization and data analysis. **a**, Polar plots of the square-rooted scattered-light intensity from the tip end for various far-field incoming beam polarizations. **b**, The far-field tip scattering is fitted with a rotated ellipse and the corresponding polarization tensor is presented. **c**, Polar plot of squared-rooted scattered-light intensity from this tip at a selected near-field position. The black arrow represents the long axis of the polar plot indicating the major axis of the highly elliptical scattered field. By back-transformation using the polarization tensor, the local-field direction can be found (red arrow). This red arrow is what we represent as a vector field in ref. 1.

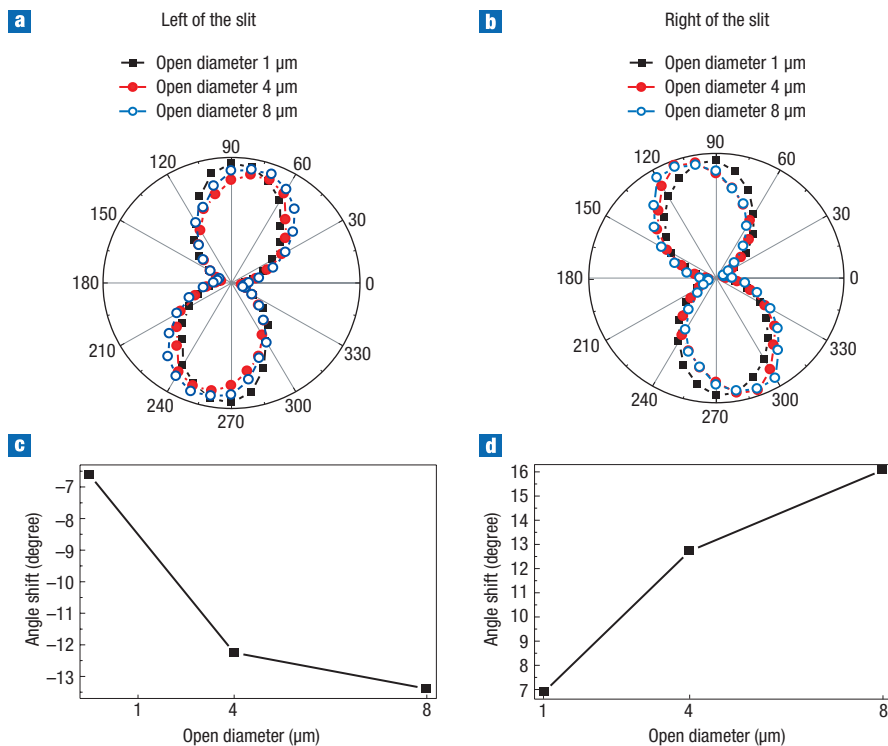


Figure 3 Background-light effect on the measured vector orientation. **a**, Polar plot of the measured intensity. A gold nanoparticle functionalized tip was located on a flat metal region on the left-hand side of the single slit used in ref. 1, about 50 μm away from the slit position where the vector field theoretically points towards the z direction. When the iris opening of the spatial filter set-up corresponds to a collection diameter of 8 μm , the experimental vector deviates from the z axis by -13.5° . Closing the iris reduces this discrepancy to -7° as shown in figures **a** and **c**. Moving the tip to the right-hand side of the slit and repeating the same experiments essentially gives the same results (**b** and **d**).

the slit. As mentioned explicitly in ref. 1, the main discrepancy is that the field on the flat metal surface is not completely oriented along the z axis. This difference mainly comes from the relatively large

background. Unlike the results shown in Figs 1 and 2 of ref. 1, which deal with mostly evanescent local fields, electric fields in the vicinity of the single slit contain both propagating and evanescent

components. Clearly this experiment is the most challenging, and in ref. 1 we have suggested that background light scattered from the shaft of the tip may be the main cause of this discrepancy, even though we have used an iris to spatially filter out this background. Any modification of the tip during the experiments is ruled out. In Fig. 3, we show additional experiments supporting this interpretation. When placing the tip in the flat metal region, we find, for an iris diameter of 8 μm , deviations from the z axis of about 15° , reducing to less than 7° when closing the iris to 1 μm . Our tip-scanning experiments had to be performed with an iris opening of 8 μm . We are highly confident that optimized scattering tips and an improved theoretical understanding of these vectorial imaging experiments will rapidly resolve these remaining discrepancies.

In conclusion, we have explicitly shown that the approach for vector-field imaging demonstrated in ref. 1 enables us to reconstruct the ellipticity of an arbitrary elliptical polarization state of the local electric field, specifically $\tan 2\psi$, $\cos(\delta_1 - \delta_2)$, a_1 and a_2 . When the tips are well characterized, our vector-field mapping is found to be largely tip-independent.

References

1. Lee, K. G. *et al.* *Nature Photon.* **1**, 53–56 (2007).
2. Gersen, H., Novotny, L., Kuipers, L. & van Hulst, N. F. *Nature Photon.* **1**, 242 (2007).
3. Born, M. & Wolf, E. *Principles of Optics* 7th edn, 28 (Cambridge Univ. Press, Cambridge, 1999).
4. Sick, B., Hecht, B. & Novotny, L. *Phys. Rev. Lett.* **85**, 4482–4485 (2000).
5. Novotny, L., Beversluis, M. R., Youngworth, K. S. & Brown, T. G. *Phys. Rev. Lett.* **86**, 5251–5254 (2001).
6. Dändliker, R., Tortora, P., Vaccaro, L. & Nesci, A. *J. Opt. A* **6**, S18–S23 (2004).

K. G. Lee¹, H. W. Kihm¹,
J. E. Kihm¹, W. J. Choi², H. Kim³,
C. Ropers⁴, D. J. Park¹, Y. C. Yoon¹,
S. B. Choi¹, D. H. Woo⁵, J. Kim⁶,
B. Lee³, Q. H. Park², Ch. Lienau⁷ and
D. S. Kim^{1*}

¹Department of Physics, Seoul National University, Seoul 151-747, Korea

²Department of Physics, Korea University, Seoul 136-701, Korea

³School of Electrical Engineering, Seoul National University, Seoul 151-747, Korea

⁴Max-Born-Institut für Nichtlineare Optik und Kurzzeitspektroskopie, D-12489 Berlin, Germany

⁵Korea Institute of Science and Technology, Seoul 136-791, Korea

⁶Korea Research Institute of Standards and Science, Taejeon 305-600, Korea

⁷Carl von Ossietzky Universität Oldenburg, Institut für Physik, D-26111 Oldenburg, Germany

*e-mail: dsk@phya.snu.ac.kr